Wind Retrieval over the Ocean using Synthetic Aperture Radar with C-band HH Polarization

Jochen Horstmann, Wolfgang Koch, Susanne Lehner, and Rasmus Tonboe

***Abstract*—The high spatial resolution and large coverage of satellite-based synthetic aperture radars (SAR) offers a unique opportunity to derive mesoscale wind fields over the ocean surface, providing high resolution wind fields near the shore. For this purpose, algorithms were developed and tested using the ScanSAR aboard the Canadian satellite RADARSAT-1, operating at C-band with horizontal polarization in transmit and receive. Wind directions are extracted from wind-induced streaks visible on most SAR images. Wind speeds are derived from normalized radar cross sections (NRCS) using empirical models. The models were developed for scatterometers (SCAT) operating at C-band with vertical polarization and must be modified for horizontal polarization. Several available C-band polarization ratios were considered, including theoretical and empirical forms. To verify and improve the algorithm, wind speeds were computed from several RADARSAT-1 ScanSAR images and compared to colocated measurements from the SCAT aboard the European remote sensing satellite ERS-2 and to the results of the Danish high resolution limited area model (HIRLAM). Using the colocated measurements, the polarization ratio was estimated and applied to improve the wind retrieval algorithm. In addition, the main error sources in SAR wind field extraction are discussed with respect to the RADARSAT-1 ScanSAR data. Sensitivity studies were performed under different atmospheric situations using the modified C-band model to compute the errors due to wind direction and inaccuracies in NRCS.**

***Index Terms*—Backscattering, ocean surface, polarization ratio, synthetic aperture radar (SAR), wind field retrieval.**

I. Introduction

OCEAN surface wind fields are computed by meteorological models and observed from satellite-based wind scatterometers (SCAT) with a resolution of the order of 50 km. Neither the models nor the SCAT give accurate wind estimates close to land because of the coarse resolution. However, to study processes in the lower atmospheric boundary layer and to get a better understanding of coastal processes, e.g., currents, waves, wind, their interaction, and related transport processes, a much finer spatial resolution is needed. The high costs of conventional ground truth measurements limits their application to small areas and short time periods.

Manuscript received September 23, 1999; revised March 30, 2000. This work was supported by the GKSS Research Center, the Deutsches Zentrum für Luft und Raumfahrt (DLR), and also by the German Bundesministerium für Bildung und Forschung (BMBF) under the ENVOC Project.

J. Horstmann and W. Koch are with the GKSS Research Center, Geesthacht, Germany.

S. Lehner is with the German Aerospace Center (DLR), DFD-AP, Oberpfaffenhofen, Germany.

R. Tonboe is with the Danish Meteorological Institute, Copenhagen, Denmark.

Publisher Item Identifier S 0196-2892(00)08914-2.

The high resolution and large spatial coverage, together with the all-weather capability of synthetic aperture radars (SAR) offer a unique opportunity to extract ocean surface wind fields. At the Danish Meteorological institute (DMI), Copenhagen, Denmark, the images acquired by the scanning SAR (ScanSAR) aboard the Canadian satellite RADARSAT-1 are the major source for the operational mapping of sea ice. Additional information on the mesoscale wind field is needed for interpretation of the images in open waters discriminated from ice infested areas and to predict the variation of the ice drift velocity [1], [2]. The ScanSAR acquires images of an area of approximately 500 km $\times$ 500 km with a spatial resolution of $\sim$100 m. It operates at 5.3 GHz (C-band) with horizontal polarization in transmitting and receiving (HH) at moderate incidence angles between 20–50°. For these incidence angles, the radar backscatter of the ocean surface is dominated by Bragg scattering from cm-scale surface roughness, which is in resonance with the incidence radiation of the radar [3], [4]. The resonant wavenumber k_r is related to the electromagnetic wavenumber k_{el} according to

$$k_r = 2k_{el} \sin\theta \tag{1}$$

where θ is the incidence angle of radar beam. This small-scale roughness is strongly influenced by the local wind field and therefore allows the radar backscatter to be a measure of wind parameters.

In the past few years, much effort has been undertaken in the derivation of wind vectors from SAR images. The wind direction can be estimated by measuring the orientation of the wind-induced streaks visible in most SAR images [5]–[7]. For wind speed retrieval, two main approaches are pursued. In the first, wind speed is estimated by measuring the normalized radar cross section (NRCS), incidence angle, and wind direction [8]–[11]. For this purpose, the NRCS must be accurately calibrated and a wind retrieval model function is required that relates the ocean surface wind speed to the NRCS, the local incidence angle of radar beam and wind direction. In the second method, wind speed is estimated from the spectral width of the image spectrum in flight direction (azimuth) [12]. For this method, a model is needed that describes the relationship between the spectral width of the azimuth spectrum, the ocean wave spectrum, and the wind speed. These methods have been applied to SAR images of the European remote sensing satellites ERS-1 and ERS-2 [13], [14]. Due to the insufficient resolution of RADARSAT-1 ScanSAR images, wind speed must be retrieved following the NRCS method taking the different polarizations into account. First attempts

using RADARSAT-1 ScanSAR images for wind speed retrieval have been performed by Thompson and Beal [15], [16] and Horstmann *et al.* [17], showing an overestimation of the wind speeds, mainly due to the lack of calibration of the ScanSAR data available at that time.

There are several empirical wind retrieval models available, which were specially developed for the ERS-1 SCAT operating at C-band with vertical polarization in transmit and receive (VV). For this work, we focus on the CMOD4 model [18]. The CMOD4 is very similar to the CMOD_IFR2 model [19], and most algorithms for C-band SAR wind retrieval are based on them. However, such well developed and verified models do not exist for the HH polarization of RADARSAT-1. Therefore a hybrid model is used which is based on the empirical C-band models and on theories and measurements of polarization ratios.

The main objective of this work is to improve and verify the wind retrieval from RADARSAT-1 ScanSAR data. Therefore, comparisons of RADARSAT-1 ScanSAR to colocated ERS-2 SCAT measurements and modeling results of the Danish high resolution limited area model (HIRLAM) were performed. In addition, the ScanSAR data allows one to study the C-band polarization ratio dependencies on incidence angles and wind speeds and to verify the HIRLAM model. A further topic is the investigation of error sources in wind retrieval from SAR. For this purpose, sensitivity studies were carried out to estimate the errors in wind speed due to inaccuracies of the NRCS and to uncertainties in wind direction with respect to RADARSAT-1 ScanSAR measurements.

II. Investigated Data Sets

The SAR images were all acquired by the Canadian Earth observation satellite RADARSAT-1 in the waters around the south part of Greenland. RADARSAT-1 operates in a near circular sun synchronous orbit at an approximate altitude of 800 km. For this study, the HH polarized C-band SAR aboard RADARSAT-1 was operated in the ScanSAR wide swath mode having the largest possible range of incidence angles between 20–50° perpendicular to flight direction. All ScanSAR data were processed by the Gatineau Processing Facility, Canada, into calibrated SAR images. A ScanSAR wide swath comprises four beams (W1, W2, W3, and S7), which cover four areas in range with sequential scans. Each processed image covers an area of approximately 500 km $\times$ 500 km with a pixel size of 50 m. The resolution of the four beams differs from 86.5–146.8 m in range and 93.1–117.5 m in azimuth. Since February 1999, the RADARSAT-1 ScanSAR beams processed at Gatineau have been calibrated with a nominal radiometric accuracy of $\pm$1.35 dB [20], although in specific areas with the occurrence of scalloping, an effect caused by a too high variation in the satellite yaw angle, calibration may degrade further. Additional calibration errors can occur due to saturation of the analog to digital convertor (ADC), which leads to a loss in signal power and in consequence to an underestimation of the NRCS. So far, radiometric calibration of ScanSAR images is extremely difficult to perform and requires considerable attention. The geometric accuracy of the ScanSAR data are in the order of approximately 100 m. The RADARSAT-1 ScanSAR data were transformed to NRCS with a calibration scheme proposed by Shepherd [21], which compensates for the scaling performed during processing and incidence angle dependencies.

The ERS-2 SCAT also operates from a circular sun synchronous orbit at C-band, although with VV polarization. The ERS-2 SCAT transmits and receives the signal at three antennae orientated at 45° forward, perpendicular, and 45° backward with respect to the satellite flight track. The ERS-2 SCAT covers incidence angles between 18–59° illuminating a swath of 500 km. The spatial resolution is $\sim$45 km, and each data area is viewed from the three directions with different incidence angles. The ERS-2 SCAT data are processed by the European Space Agency (ESA), Noordwijk, The Netherlands, to wind fields using the C-band model CMOD4. The resulting wind field is available on a grid of 25 km $\times$ 25 km covering a 500 km wide swath along the orbit.

HIRLAM is a mesoscale atmospheric model that is operational at the DMI. It is a semi-implicit model, with Eulerian advection and leap frog time stepping (details are provided by Gustafsson [22] and Wolters *et al.* [23]). For the Greenland area, it was set up with a time step of 240 s and a horizontal resolution of 0.45°. The analysis of the model is performed every 6 h using the optimum interpolation method, which is a statistical procedure to minimize the difference between observations and first guess from the model. The lateral boundary values for the model are obtained from the global European Center for Medium Range Weather Forecast (ECMWF) model.

For this study, ten RADARSAT-1 ScanSAR images of the ocean surface were collected around Cape Farewell, located at the southern tip of Greenland (59–61°N, 38–48°E between January and August 1999 at $\sim$2030 UTC. For five of the ScanSAR images, colocated ERS-2 SCAT wind fields were available, all acquired at $\sim$0100 UTC approximately 4.5 h after the ScanSAR image. Results of the HIRLAM model were available for all the images. The HIRLAM data were available at 2100 UTC as 3-h forecast retrieved from the 1800 UTC analysis and fit the time of ScanSAR acquisition quite well.

III. SAR Wind Retrieval

The wind direction can be derived from the orientation of wind-induced streaks, such as boundary layer rolls in the atmosphere, visible in most SAR images [7]. Therefore SAR subimages are transformed into the wavenumber domain, where the wind direction corresponds to the direction perpendicular to the line connecting the maxima of spectral energy. A spectral filter is applied for wave lengths between 500–1500 m to distinguish wind-induced stripes from ocean waves and from larger scale atmospheric structures such as atmospheric gravity waves. Due to the symmetry of the spectrum, the wind direction can only be computed with a 180° ambiguity. The algorithm shows good results applied to ERS-1 and ERS-2 SAR images [7], [24]. However, application of the method to RADARSAT-1 ScanSAR images failed in many cases. This is mainly due to the inadequate spatial resolution of the images. Therefore, the additional use of other information such as atmospheric models, weather charts,

or measurements are recommended when using RADARSAT-1 ScanSAR images.

For derivation of wind speeds from SAR images, the local NRCS, incidence angle of radar beam, and wind direction with respect to the antenna look direction are needed as input into our algorithm. The algorithm is based on the inversion of a C-band model function relating the NRCS of the ocean surface σ_0 to wind speed u and wind direction versus look direction ϕ according to

$$\sigma_0^{pol} = au^{\gamma}(1 + b\cos\phi + c\cos 2\phi) \tag{2}$$

where a, b, c, and γ are coefficients that in general depend on radar frequency, polarization, and incidence angle. These coefficients were determined empirically in the cases of the model functions CMOD4 and CMOD_IFR2 by evaluation of ERS-1 SCAT data and wind fields from the ECMWF. For the CMOD_IFR2 model, buoy measurements of the National Oceanic and Atmospheric Administration (NOAA), Washington, DC, were considered in addition. Both models have been applied successfully to ERS-1 and ERS-2 SAR images [10], [6], [5], [11]. So far there are no similarly well-developed and validated C-band models for HH polarization available so that the models previously discussed had to be modified using the C-band polarization ratio. In the range of moderate incidence angles (20–70°), the backscatter for VV polarization is larger than for HH polarization [25]. The C-band polarization ratio has been measured with an airborne SCAT by Unal *et al.* [26] for incidence angles of 20°, 30°, and 45° for wind speeds from 2–14 ms^{-1}. Their work shows that the ratio, defined as VV/HH hereafter, is mainly dependent on incidence angles, and for wind speeds below 6 ms^{-1}, a wind speed dependency was also observed. Thompson *et al.* [27] proposed a polarization ratio model independent of wind speed and fitted the model to the data of [26]. The model has the following form:

$$\sigma_0^{\mathrm{HH}} = \frac{(1 + \alpha\tan^2\theta)^2}{(1 + 2\tan^2\theta)^2}\,\sigma_0^{\mathrm{VV}}(u, \phi, \theta). \tag{3}$$

Here, σ_0^{HH} is the HH polarized NRCS, σ_0^{VV} is the VV polarized NRCS, θ is the incidence angle, and α is a constant which was set to 0.6, fitting the data of Unal *et al.* [26] quite well. Changing α in (3) to 0 gives the theoretical polarization ratio for Bragg scattering, and setting α to 1 results in Kirchhoff scattering. The basic assumption of Kirchhoff scattering is that the plane-boundary reflection occurs at every point on the surface [28], [29]. A further model was suggested by Elfouhaily [30]

$$\sigma_0^{\mathrm{HH}} = \frac{(1 + 2\sin^2\theta)^2}{(1 + 2\tan^2\theta)^2}\,\sigma_0^{\mathrm{VV}}(u, \phi, \theta). \tag{4}$$

The polarization ratios of (3) with α of 0 (Bragg scattering), 0.6, and 1 (Kirchhoff scattering) are plotted in Fig. 1 together with the ratio of (4).

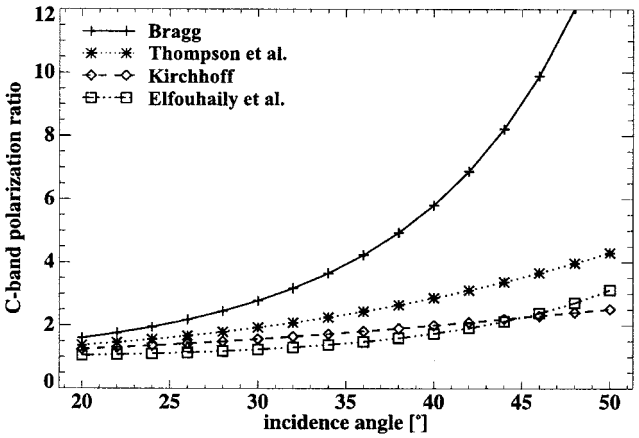

Fig. 1. C-band polarization ratios are plotted versus incidence angles using the model functions from (3) and (4).

IV. Comparison of Wind Speeds From ScanSAR to ERS-2 SCAT

For a first comparison, the RADARSAT-1 ScanSAR scene acquired on April 21, 1999 at 2037 UTC showing the area and ocean surface around the south part of Greenland was used. Along the east coast of Greenland, a 20–30 km wide ice belt is clearly visible (Fig. 2), which is known to flow southward around Cape Farewell into the Julianehaab Bay situated at the southwest coast of Greenland. Most of the area in the Julianehaab Bay is also covered by sea ice, which opens up to the west of the bay. According to the analyzed weather charts, there are easterly winds with low wind speeds that increase toward the south. Furthermore, there is a wind front just south of Cape Farewell which can be seen in the image. Southwest of Cape Farewell there are streaks visible in the ScanSAR image which are due to wind and indicate the mean wind direction in the area ($\sim$65°).

Wind speeds over the ocean surface were computed from the ScanSAR data using the hybrid model function composed of the CMOD4 model and polarization ratio according to Thompson *et al.* [27]. To reduce the effect of speckle, discussed in Section VI, the NRCS and incidence angles of the ScanSAR image were averaged over 2 km $\times$ 2 km. For this comparison, the wind direction was set to 75°, which is the mean wind direction retrieved from the colocated ERS-2 SCAT measurements acquired 4.5 h later varying between 59–89°. The mean wind direction agrees well with the mean orientation of the large scale streaks visible in the ScanSAR image and to the wind direction from the weather chart. Fig. 2 shows a wind speed map where the color scale of the image represents wind speeds between 0–20 ms^{-1} as computed from the ScanSAR data. Corresponding wind speeds measured from the ERS-2 SCAT are represented by superimposed squares in the same color scale. Over the entire image, the ScanSAR derived wind speeds are significantly higher than the measurements from ERS-2 SCAT. The decrease of wind speed in the near range of the image (0–70 km) is an artifact observed in most investigated ScanSAR images and is most likely due to ADC saturation which occurs especially in near range at high wind speeds. Also at a distance of 392 km in range, a nadir range ambiguity line (a SAR artifact) is observed over the entire flight direction. However, it is obvious that the relative wind variation over the whole region has the same trend for both sensors which shows that ScanSAR is capable of mapping small scale variations.

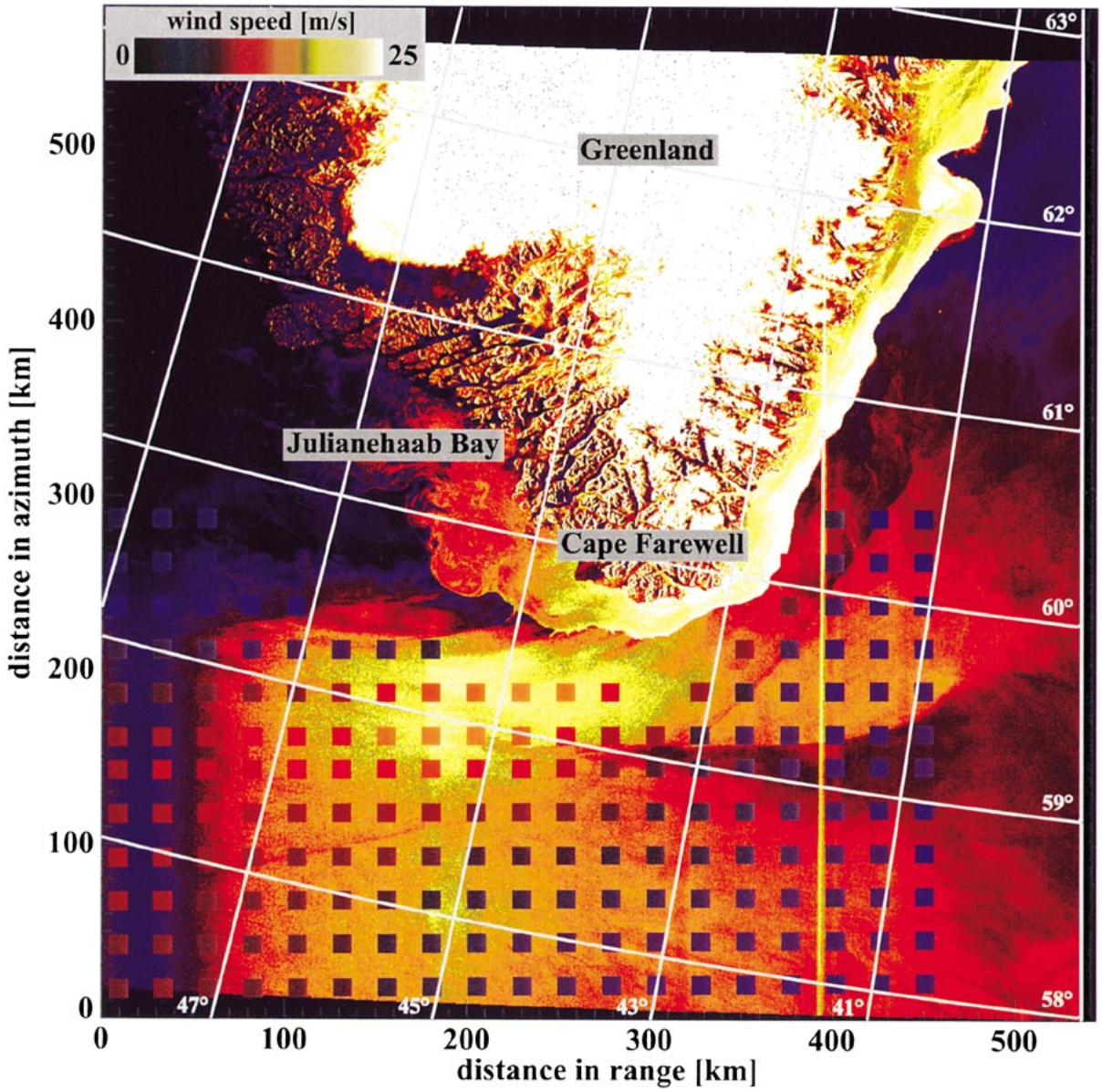

Fig. 2. Wind speed map extracted from the scanning synthetic aperture radar (ScanSAR) wide swath data of the Canadian satellite RADARSAT-1. The image was acquired on April 21, 1999 at 2035 UTC, showing the area around the south part of Greenland. The color scale of the image gives the wind speed which was computed from the ScanSAR data with a fixed wind direction of 75°, using the hybrid model function composed of the CMOD4 and the polarization ratio according to Thompson *et al*. The color scale of the superimposed squares represent the wind speeds measured by the scatterometer (SCAT) aboard the European Remote Sensing satellite ERS-2 approximately 4.5 h later. © Danish Meteorological Institute and RADARSAT International.

In a next step, wind speeds from ScanSAR and ERS-2 SCAT are compared point by point on the same grid. For this purpose, the NRCS and incidence angles of the RADARSAT-1 ScanSAR images are averaged over 25 km $\times$ 25 km on the grid used by the ERS-2 SCAT. The ScanSAR NRCS and incidence angles are used together with the wind direction from the corresponding ERS-2 SCAT grid cell as input to the hybrid model function to derive the wind speed. In Fig. 3, the resulting ScanSAR wind speeds are plotted versus the corresponding ERS-2 SCAT wind speeds. The stars represent the results of grid cells which are open water dominated by the wind while the squares are associated to grid cells which are affected by other ocean surface features, i.e., sea ice. The main statistical parameters of this plot are listed in Table III. The correlation is 0.65 and the bias of 3.69 ms^{-1} shows that wind speeds computed from ScanSAR are significantly higher than the measurements from ERS-2 SCAT. The comparison indicates an error in the applied transfer function which is most likely due to the choice of C-band polarization ratio. According to these results, the polarization ratio is overestimated, making the estimated wind speed too high. To get an estimate of the polarization ratio and its dependencies, the NRCS for VV polarization has to be computed at each point of the RADARSAT-1 ScanSAR image. At each point of the grid, the ERS-2 SCAT wind speed and wind direction measurement are put together with the ScanSAR incidence angles as input to the CMOD4 model, which then gives an estimate of the VV polarized NRCS. Taking the corresponding NRCS from the ScanSAR HH polarized data the VV/HH polarization ratio of each grid cell is derived.

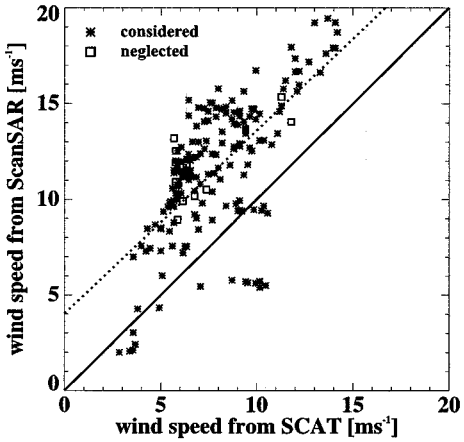

Fig. 3. Scatter plot of wind speeds retrieved from the RADARSAT-1 ScanSAR image from April 25, 1999, and the colocated ERS-2 SCAT data acquired 4.5 h later. Wind speeds from ScanSAR were computed with the hybrid model function consisting of the CMOD4 and the polarization ratio according to the model of Thompson *et al.* As input to the hybrid model, the NRCS and incidence angles were taken from the ScanSAR data and the wind direction from the ERS-2 SCAT measurements. The stars represent measurements of the areas where the backscatter was dominated by the wind, while the squares indicate data that were neglected mainly due to the presence of sea ice. The dotted line gives the regression of all considered points denoted by the stars.

TABLE I
STATISTICAL PARAMETERS OF THE COMPARISON OF THE SCATTER PLOT SHOWN IN FIG. 3

	comparison	
bias [ms^{-1}]	3.69	
correlation	0.65	
RMS error [ms^{-1}]	4.61	
scatter [%]	57.8	
nr. of samples	324	
	ScanSAR	ERS-2 SCAT
mean [ms^{-1}]	11.66	7.98
std. dev. [ms^{-1}]	3.64	2.47
maximum [ms^{-1}]	19.5	14.2

For the ten ScanSAR scenes, five colocated ERS-2 SCAT measurements were available, and for each of the five scenes the corresponding weather charts were analyzed with respect to the development of the weather situation between acquisition of the ScanSAR and ERS-2 SCAT data. The analysis of the weather charts for January 30, 1999 shows very high wind speeds up to 30 ms^{-1} (beyond the limits of calibration of CMOD4) and strong changes in wind speed and direction with time so that these data were omitted in the investigations. Data of four ScanSAR scenes and their colocated ERS-2 SCAT data where considered, which cover a wide range of wind speeds, wind directions, and incidence angles.

In Fig. 4, the resulting VV/HH polarization ratio is plotted versus incidence angle between 20–50° and in Fig. 5 versus wind speed. Again, stars represent results of areas where the backscatter is dominated by the wind, and the squares indicate data that were strongly affected by features not caused by the

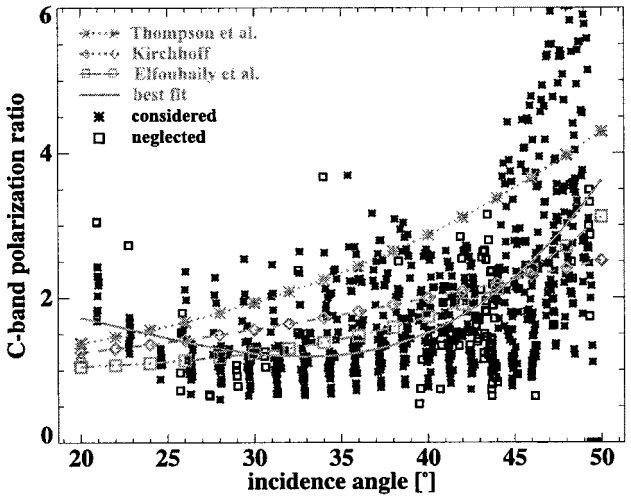

Fig. 4. Dependency of the C-band VV/HH polarization ratio on incidence angles. The HH polarized NRCS is derived from the RADARSAT-1 ScanSAR image. Taking the wind speed and direction from ERS-2 SCAT together with the incidence angle from the RADARSAT-1 ScanSAR data, the VV polarized NRCS is derived using the CMOD4 model.

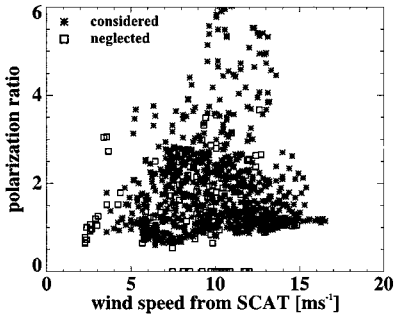

Fig. 5. Dependency of the C-band VV/HH polarization ratio on wind speed derived as in Fig. 4.

wind. For comparison the theoretical polarization ratio dependencies and the best fit are plotted. There is a significant change of polarization ratio over the entire range of incidence angles. In the near range of the image (20–30°), a decrease of polarization ratio with incidence angles is observed that does not agree with the theoretical ratios. For incidence angles between 30–40°, the ratio is nearly constant, and for larger incidence angles, a distinct increase of polarization ratio is seen. The decrease of polarization ratio in near range cannot be explained by the theoretical approaches and is most likely due to ADC saturation, already observed earlier in this paper. For higher incidence angles, the polarization ratio shows the same trend as from Kirchhoff scattering and as the approach of Elfouhaily [30]. Similar results were observed by Vachon *et al.* [31], who fitted α in (3) to $\sim$1.2 for incidence angles between 20–48°, using well calibrated RADARSAT-1 SAR images. From the plot of Fig. 5, no dependency on wind speed can be resolved. However, the large scatter indicates that another parameter dominates the dependency on polarization ratio. According to the previous observation, the model proposed by Thompson *et al.* [27] overestimates the polarization ratio resulting in too high wind speeds from ScanSAR. For that reason, the comparison of the four ScanSAR

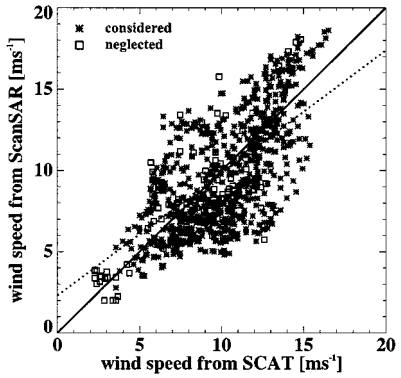

Fig. 6. Wind speeds derived from four ScanSAR images versus the corresponding ERS-2 SCAT data. Wind speeds from ScanSAR were computed with the hybrid model function consisting of the CMOD4 and the polarization ratio according to Kirchhoff scattering. As input to the model, the NRCS and incidence angles were taken from the ScanSAR data and the wind direction from the ERS-2 SCAT measurements. Stars represent results from areas that were mainly influenced by the wind. Squares represent results that were strongly affected by sea ice or other phenomena. The dotted line gives the regression of all considered points denoted by the stars.

TABLE II
STATISTICAL PARAMETERS FROM COMPARISON BETWEEN WIND SPEED FROM FOUR SCANSAR SCENES AND THE COLOCATED ERS-2 SCAT MEASUREMENTS

	comparison	
bias [ms^{-1}]	-0.08	
correlation	0.62	
RMS error [ms^{-1}]	2.72	
scatter [%]	28.0	
nr. of samples	883	
	ScanSAR	ERS-2 SCAT
mean [ms^{-1}]	9.6	9.7
std. dev. [ms^{-1}]	3.36	2.78
maximum [ms^{-1}]	18.6	16.5

images to ERS-2 SCAT measurements is performed using the polarization ratio given by the Kirchhoff scattering model. The wind speeds from ScanSAR were computed using the NRCS and incidence angle from ScanSAR together with the wind direction of each corresponding ERS-2 SCAT measurement as input to the hybrid model. In Fig. 6, the scatter plot is shown of 1023 colocated samples, of which 240 were neglected due to sea ice or significant calibration errors visible in the image (at kilometer 392 in range). The corresponding main statistical parameters are listed in Table II. Although the ScanSAR and ERS-2 SCAT data are acquired 4.5 h apart the results are in fair agreement, having a correlation of 0.62 with nearly no bias. These results show the applicability of RADARSAT-1 ScanSAR for wind speed retrieval, though efforts for better calibration have to be undertaken.

V. COMPARISON OF SCANSAR TO HIRLAM

To test the applicability of the hybrid model function for a large range of wind situations, a comparison was performed using a larger data set. In the Cape Farewell area, ten ScanSAR scenes were acquired between January and August 1999 that were processed at Gatineau, PQ, Canada, having an acceptable accuracy of the NRCS for the purpose of wind speed retrieval. All images were acquired at approximately 2030 UTC and compared to the HIRLAM forecast of 2100 UTC. Again, the ScanSAR scene from January 30, 1999 was omitted due to the high wind speeds that are beyond the limits of applicability of the CMOD4. For this comparison, the ScanSAR images were averaged to the grid of HIRLAM, resulting in an average grid cell size of approximately 28 km $\times$ 55 km. Again, wind speeds were retrieved from ScanSAR using the hybrid model function. The comparison was performed considering the polarization ratio according to Kirchhoff scattering and the best fit retrieved in Section IV from ScanSAR and the corresponding ERS-2 SCAT measurements (Fig. 4). For each grid cell, the wind speeds were derived using the NRCS and incidence angle from the ScanSAR, together with the wind direction from the HIRLAM model. In Fig. 7, wind speeds retrieved from ScanSAR, assuming the polarization ratio according to Kirchhoff scattering, is plotted versus wind speed from HIRLAM. The same scatter plot is shown in Fig. 8, where the polarization ratio resulting from the best fit was used for wind speed retrieval. Both plots look very alike, though the scatter of Fig. 8 is lower. In Table III, the main statistical parameters are listed for

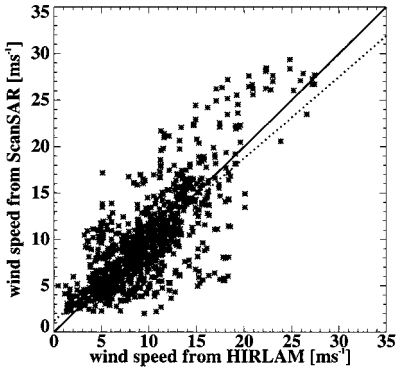

Fig. 7. Wind speeds retrieved from nine RADARSAT-1 ScanSAR images are plotted versus the corresponding wind speeds resulting from the HIRLAM model. Wind speeds were computed with the hybrid model function considering the polarization ratio according to Kirchhoff scattering. As input to the model, the NRCS and incidence angles were taken from the ScanSAR data and the wind direction from the HIRLAM model. The dotted line gives the regression of all considered points denoted by the stars.

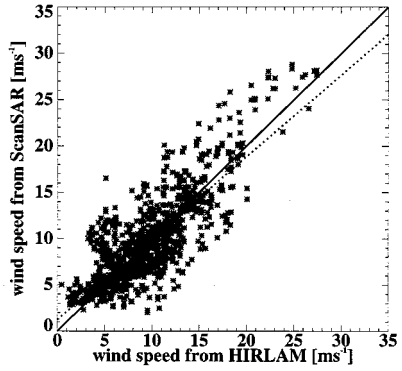

Fig. 8. Same as in Fig. 7, except that the polarization ratio according to the best fit from Fig. 7 was used in the hybrid model.

TABLE III
STATISTICAL PARAMETERS FROM COMPARISON BETWEEN WIND SPEEDS FROM NINE RADARSAT-1 SCANSAR IMAGES AND RESULTS OF THE HIRLAM MODEL. WIND SPEEDS FROM SCANSAR WERE RETRIEVED CONSIDERING THREE DIFFERENT POLARIZATION RATIOS, ACCORDING TO KIRCHHOFF SCATTERING, MODEL OF ELFOUHAILY *et al.*, AND BEST FIT FROM FIG. 4 UPPER PLOT

	Kirchoff scattering	Elfouhaily et al.	best fit	
bias [ms^{-1}]	0.01	-0.84	0.07	
correlation	0.75	0.74	0.80	
RMS error [ms^{-1}]	3.41	3.46	2.94	
scatter [%]	34.9	35.4	30.0	
nr. of samples	1073	1073	1073	
	ScanSAR	ScanSAR	ScanSAR	HIRLAM
mean [ms^{-1}]	9.79	8.94	9.84	9.77
std. dev. [ms^{-1}]	5.11	4.84	4.82	4.38
maximum [ms^{-1}]	29.4	29.1	28.8	27.4

the comparison of wind speed assuming the polarization ratios according to Kirchhoff scattering, model of Elfouhaily, and the best fit. The correlations of the comparison between ScanSAR and HIRLAM is for all of the three ratios $\geq$0.74 and significantly better than the correlation of 0.62 resulting from the comparison to ERS-2 SCAT. This is most likely due to changes of the wind situation in the 4.5 h time difference. However, the results using the two polarization models are quite similar, and we cannot conclude which model is better. Comparison of the applied polarization ratios show significantly better coincidence between ScanSAR and HIRLAM winds when using the ratio retrieved from the best fit.

In the next step, the difference in wind speed between ScanSAR and HIRLAM is derived for each ScanSAR image at every grid cell. The results are coded in grey levels and plotted at its location in the ScanSAR image. In Fig. 9, the ScanSAR image acquired on April 21, 1999 is shown. The grey scale of the image represents the NRCS of the ScanSAR data, and the grey scale of the superimposed squares represents the difference in wind speed between ScanSAR and HIRLAM. The main differences in wind speed occur in near range of the image (between 0–70 km), in the lee of the coast, and near to the front (indicated by the white arrows). The first is most likely due to calibration inaccuracies in near range. However, the other two phenomena cannot be caused by calibration errors or a wrong choice of the transfer function. In eight of the ten studied ScanSAR images, the wind speed in near range was significantly underestimated. In all images, distinct differences in wind speed were observed near the coast, especially in the presence of wind shadowing, which shows that ScanSAR can significantly improve the information on the wind field, especially in such unattainable areas.

VI. ERROR ESTIMATION

When computing wind speeds from ScanSAR with the C-band hybrid model function, the accuracy is strongly dependent on the inputs to the algorithms, NRCS, wind direction, and incidence angle. The error in wind speed due to error in incidence angle is negligible because it can be computed very precisely from the ScanSAR data. Main errors are caused by the

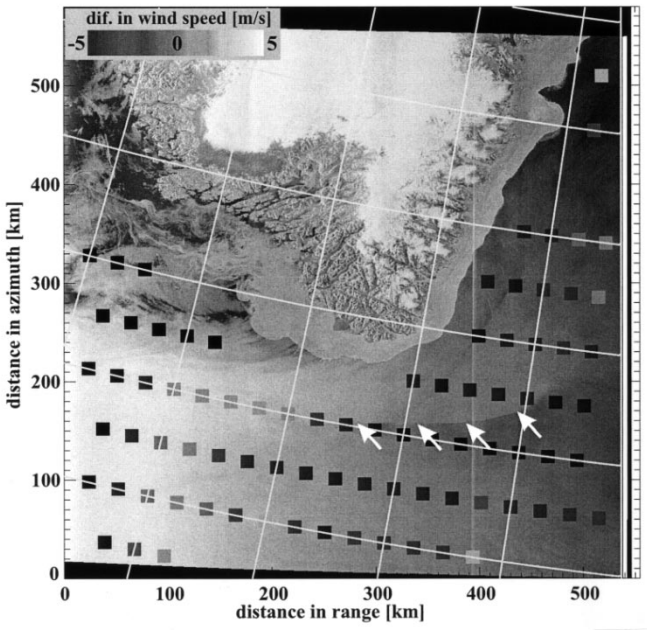

Fig. 9. RADARSAT-1 ScanSAR image acquired on April 21, 1999. The image represents the NRCS of the ScanSAR data, and the grey scale of the superimposed squares represents the difference in wind speed between ScanSAR and HIRLAM. The white arrows point at a front imaged by the ScanSAR. ©Danish Meteorological Institute and RADARSAT International.

effect of speckle, uncertainty in wind direction, and calibration accuracy of NRCS. The granular appearance of SAR images is the effect of speckle. It is a small-scale fluctuating component of the backscatter [32] and is attributed to interference effects that occur from scattering of coherent electromagnetic waves by rough surfaces. In the case of RADARSAT-1 ScanSAR images, the backscatter variation caused by speckle can be up to $\pm$3 dB on a single pixel. For ScanSAR images, the variance of NRCS for grid cell sizes below 2 km is primarily caused by speckle and therefore should not be interpreted as wind variation. To reduce the effect of speckle, the NRCS of the images must be averaged over at least 2 km $\times$ 2 km.

More important is the necessity to have information on wind direction for retrieval of the wind speed. The NRCS is strongly dependent on wind direction and therefore, uncertainties in wind direction can lead to significant errors in wind speed. The relative error in wind speed is plotted in Fig. 10 assuming an uncertainty in wind direction of $\pm$10°. The computations were performed for incidence angles of 20°, 35°, and 50°, using the CMOD4 with the Kirchhoff model polarization ratio. The error is plotted for wind speeds between 2–30 ms^{-1}, and wind directions from 0° (upwind) to 180° (downwind) clockwise from radar look direction. The largest relative errors result from wind directions near to 45° and 135°, respectively, and near to 225° and 315°, due to the symmetry of the hybrid model function. With increasing incidence angles and for low wind speeds, the error increases, although for higher wind speeds, there is a distinct decrease of error with increasing incidence angles.

The error in wind speed due to the accuracy of the NRCS is strongly dependent on the sensor performance and its calibration. In Fig. 11, the error in wind speed is plotted assuming an accuracy of $\pm$0.5 dB. The computations were performed with

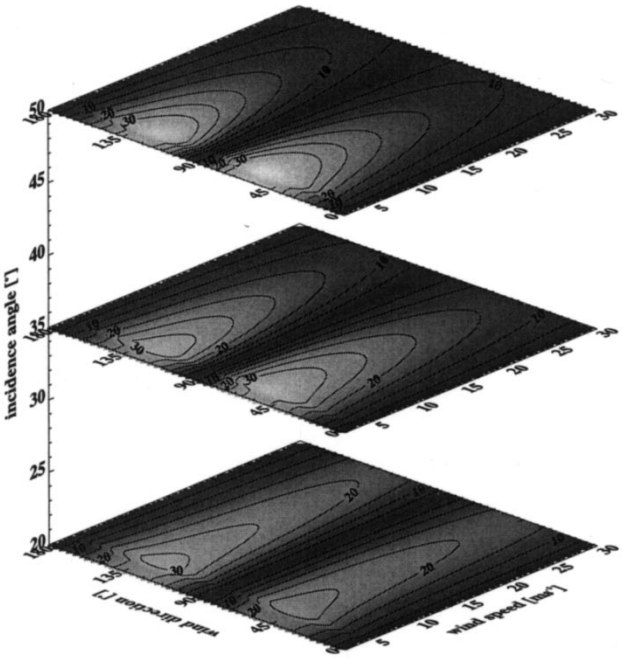

Fig. 10. Computed relative error in percentage of wind speed due to an uncertainty in wind direction of $\pm 10°$ for incidence angles of 20°, 35°, and 50°. The error was computed for wind speeds between 2–30 ms^{-1} and wind directions from 0 to 180°.

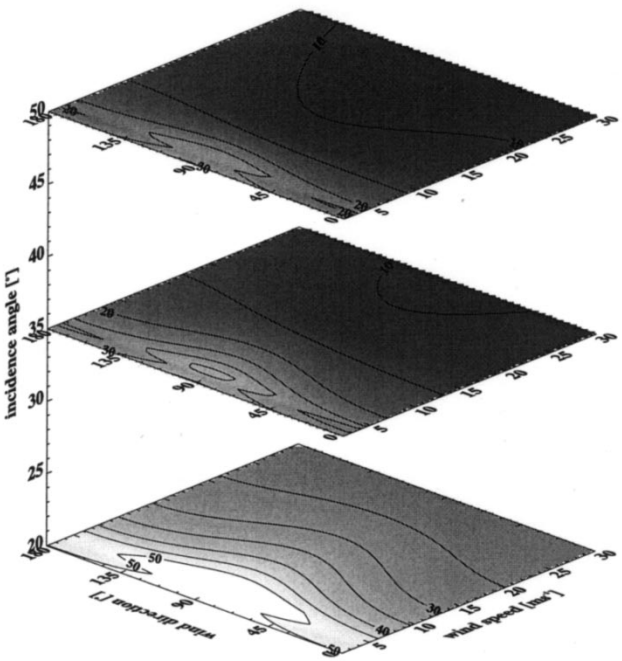

Fig. 11. Computed relative error in percentage of wind speed due to an uncertainty in NRCS of ± 0.5 dB for incidence angles of 20°, 35°, and 50°. The error was computed for wind speeds between 2–30 ms^{-1} and wind directions from 0 to 180°.

the same model and the same ranges of input parameters used for the results of Fig. 10. The relative error decreases significantly with increasing wind speed and is slightly lower for cross wind than for up- and downwind. This behavior also occurs for increasing incidence angles, though the error decreases significantly with increasing incidence angle. However note, that in case of RADARSAT-1 ScanSAR the error of NRCS can increase significantly, e.g., in near range due to power loss and at the range ambiguity lines.

VII. Conclusions

In this paper, a hybrid model function was presented and tested to derive wind speeds from calibrated C-band HH polarized RADARSAT-1 ScanSAR images. The hybrid model function is based on the C-band model CMOD4, which was developed for VV polarized ERS-1 SCAT, and an additional term that includes the polarization ratio. To improve and validate the algorithm, a data set was collected around the south part of Greenland consisting of ten RADARSAT-1 ScanSAR images, colocated results of the 2100 UTC forecasts of HIRLAM and five colocated ERS-2 SCAT measurements. Using the ScanSAR and ERS-2 SCAT measurements, which were acquired 4.5 h later, the polarization ratios were derived and their dependency on incidence angle and wind speed were investigated. The best fitting theoretical polarization ratios were according to Kirchhoff scattering and an extended model proposed by Elfouhaily *et al.* [30]. However, there were significant differences between the empirical estimated and the theoretical polarization ratios, so a ratio was fitted to these data. Using the CMOD4 in combination with the polarization ratio according to Kirchhoff scattering, wind speeds were derived from ScanSAR and compared to ERS-2 SCAT measurements. An overall correlation of 0.62 was found and ScanSAR retrieved wind speeds were especially overestimated at high wind speeds (> 13 ms^{-1}). A further comparison was performed with the colocated HIRLAM data using the hybrid model function with the polarization ratios according to Kirchhoff scattering, the model suggested by Elfouhaily [30], and to the best fit, respectively. The resulting correlations were 0.75, 0.74, and 0.80 with a bias of 0.01, -0.84, and 0.07 ms^{-1}. Investigation of the location of the largest deviations between ScanSAR and HIRLAM results showed a significant underestimation of the shadowing effect of Greenland by the HIRLAM model and distinct calibration inaccuracies in the ScanSAR data especially at near range (0–70 km), which are most likely caused by ADC saturation. Overall calibration of RADARSAT-1 ScanSAR data still requires particular attention to compute accurate wind fields over the ocean surface.

Errors in wind speed due to uncertainty of wind direction and inaccuracies in NRCS were estimated for different incidence angles, wind speeds, and wind directions. The main errors in wind speed due to uncertainties in wind direction occur near to wind directions of 45° and 135°, respectively, and near to 225° and 315°. This is simply due to the azimuthal behavior of CMOD4, with changes in wind speed with wind directions around the given directions relative to the antenna look direction. The relative error caused by inaccuracies of the NRCS decreases significantly with increasing wind speed and is slightly lower for cross wind than for up- and downwind. So far, radiometric calibration is the main error source when retrieving wind speeds from RADARSAT-1 ScanSAR data, especially at high wind speeds in the near range of the image, where ADC saturation can occur.

The error of wind speed caused by speckle reduces significantly with increasing area of averaging and therefore the wind speed resolution should be in the order of 2 km $\times$ 2 km. In combination with wind directions from the HIRLAM model, wind speed errors due to errors in estimated wind direction can be kept small.

Overall, the investigation shows the applicability of RADARSAT-1 ScanSAR images for mesoscale wind speed retrieval over the ocean surface. Their large coverage, together with their high resolution of 2 km $\times$ 2 km, gives valuable additional information on wind fields and their variation, especially near coasts. Although calibration is so far insufficient, the method in its present form can help analyze and improve results of atmospheric models especially near to the coast. For the case of the images under investigation, it was shown that HIRLAM underestimates (probably due to insufficient resolution of the topography) the shadowing effect behind Greenland. The operational use of RADARSAT-1 ScanSAR wind maps retrieved from the hybrid model function, together with the wind directions from HIRLAM, is planned at the Danish Meteorological Institute to help improve weather and especially ice drift forecast in the area around Greenland.

The advanced SAR (ASAR) aboard the Environmental Satellite (ENVISAT), scheduled for launch in June 2001, will be capable of operating at wide swath mode as well but with choice of polarization. This will enable to investigate the polarization ratio in more detail and help improve wind retrieval from SAR. Therefore, the algorithm and methods developed in this study are an ideal preparation for the ENVISAT era.

ACKNOWLEDGMENT

The ERS-2 SCAT data were kindly provided by the European Space Agency (ESA), Noordwijk, The Netherlands, as part of the BIGPASO project which is worked on in close collaboration of GKSS, Geesthacht, Germany, German Aerospace Center (DLR), Oberpfaffenhofen, Germany, and the Danish Meteorological Institute (DMI), Copenhagen, Denmark.

REFERENCES

[1] R. S. Gill, M. K. Rosengreen, H. S. Andersen, R. T. Tonboe, and H. H. Valeur, "Sea ice mapping around Greenland using Radarsat," in *Proc. 7th Int. Conf. Development and Commercial Utilization of Technologies in Polar Regions*, Nuuk, Greenland, 1998.

[2] R. T. Tonboe, R. S. Gill, and J. Horstmann, "Near ice edge estimation of the sea surface winds using Radarsat ScanSAR," in *Proc. 1999 EUMETSAT Meteorological Satellite Data Users Conf.*, Copenhagen, Denmark, 1999.

[3] J. W. Wright, "Backscattering from capillary waves with applications to sea clutter," *IEEE Trans. Antennas Propagat.*, vol. AP-14, pp. 749–754, 1966.

[4] G. R. Valenzuela, "Theories for the interaction of electromagnetic and oceanic waves—A rewiev," *Bound. Layer Metereol.*, vol. 13, pp. 61–85, 1978.

[5] P. W. Vachon and F. W. Dobson, "Validation of wind vector retrieval from ERS-1 SAR images over the ocean," *Global Atmos. Ocean Syst.*, vol. 5, pp. 177–187, 1996.

[6] C. C. Wackerman, C. L. Rufenach, R. Schuchman, J. A. Johannessen, and K. Davidson, "Wind vector retrieval using ERS-1 synthetic aperture radar imagery," *J. Geophys. Res.*, vol. 34, pp. 1343–1352, 1996.

[7] S. Lehner, J. Horstmann, W. Koch, and W. Rosenthal, "Mesoscale wind measurements using recalibrated ERS SAR images," *J. Geophys. Res.*, vol. 103, pp. 7847–7856, 1998.

[8] W. Alpers and B. Brümmer, "Atmospheric boundary layer rolls observed by the synthetic aperture radar aboard the ERS-1 satellite," *J. Geophys. Res.*, vol. 99, pp. 12 613–12 621, 1994.

[9] W. Rosenthal, S. Lehner, J. Horstmann, and W. Koch, "Wind measurements using ERS-1 SAR," in *Proc. 2nd ERS Applications Workshop*, London, U.K., 1995, pp. 355–358.

[10] A. Scoon, I. S. Robinson, and P. J. Meadows, "Demonstration of an improved calibration scheme for ERS-1 SAR imagery using a scatterometer wind model," *Int. J. Remote Sensing*, vol. 17, no. 2, pp. 413–418, 1995.

[11] J. Horstmann, "Untersuchung zur windgeschwindigkeitsbestimmung aus dem radar mit synthetischer apertur ann bord der ERS-1/2 satelliten," GKSS Rep. GKSS 97/E/55, ISSN 0344-9629, Geesthacht, Germany, 1997.

[12] B. Chapron, T. Elfouhaily, and V. Kerbaol, "A SAR speckle wind algorithm," in *Proc. 2nd ERS-1 Workshop*. Plouzane, France: l'Inst. Français Rec. l'Exploitation Mer (IFREMER), 1994.

[13] V. Kerbaol, B. Chapron, and P. W. Vachon, "Analysis of ERS-1/2 synthetic aperture radar wave mode imagettes," *J. Geophys. Res.*, vol. 103, pp. 7833–7846, 1998.

[14] S. Lehner, J. Schulz-Stellenfleth, B. Schättler, H. Breit, and J. Horstmann, "Wind and wave measurements using complex ERS-2 SAR wave mode data," *IEEE Trans. Geosci. Remote Sensing*, vol. 38, pp. 2246–2257, Sept. 2000.

[15] D. R. Thompson and R. C. Beal, "Mapping mesoscale and submesoscale wind fields using synthetic aperture radar," in *Proc. Int. Geoscience and Remote Sensing Symp. 1998*, Seattle, WA, 1998.

[16] ——, "Mapping of mesoscale and submesoscale wind fields using synthetic aperture radar," *Appl. Phys. Lab. Tech. Dig.*, vol. 21, no. 1, pp. 58–67, 1999.

[17] J. Horstmann, W. Koch, S. Lehner, and R. Tonboe, "Computation of wind vectors over the ocean using spaceborne synthetic aperture radar," *Appl. Phys. Lab. Tech. Dig.*, vol. 21, no. 1, pp. 100–107, 1999.

[18] A. Stoffelen and D. Anderson, "Scatterometer data interpretation: Estimation and validation of the transfer function CMOD4," *J. Geophys. Res.*, vol. 102, pp. 5767–5780, 1997.

[19] Y. Quilfen and A. Bentamy, "Calibration/validation of ERS-1 scatterometer precision products," in *Proc. Int. Geoscience and Remote Sensing Symp. 1994*, Pasadena, CA, 1994, pp. 945–947.

[20] S. K. Srivastava, B. T. Banik, M. Adamovic, and R. Gray, "Maintaining image quality and calibration of RADARSAT-1 CDPF products," in *Proc. Int. Geoscience and Remote Sensing Symp. 1999*, Hamburg, Germany, 1999, pp. 443–445.

[21] N. Shepherd, "Extraction of beta nought and sigma nought from RADARSAT CDPF products," Rep. AS97-5001 Rev. 2, Can. Space Agency, Ottawa, ON, Canada, 1998.

[22] N. Gustafsson, "HIRLAM 2 Final Rep.: HIRLAM Tech. Rep. 9," Swedish Meteorol. Hydrol. Inst., Norrkoeping, Sweden, 1994.

[23] L. Wolters, G. Cats, N. Gustafsson, and T. Wilhelmsson, "Data-parallel numerical methods in a weather forecast model," *Appl. Numer. Math.*, vol. 19, pp. 159–171, 1995.

[24] J. Horstmann, I. Weinreich, D. Hauser, S. Lehner, and W. Koch, *SAR Wind Measurements During the FETCH Experiment*. Amsterdam, The Netherlands: Elsevier, 1999.

[25] H. Masuko, K. Okamoto, M. Shimada, and S. Niwa, "Measurement of microwave backscattering signatures of the ocean surface using X band and K_α band airborne scatterometers," *J. Geophys. Res.*, vol. 91, no. C11, pp. 13 065–13 083, 1986.

[26] C. M. H. Unal, P. Snooji, and P. J. F. Swart, "The polarization-dependent relation between radar backscatter from the ocean surface and surface wind vectors at frequencies between 1 and 18 GHz," *IEEE Trans. Geosci. Remote Sensing*, vol. 29, pp. 621–626, 1991.

[27] D. R. Thompson, T. M. Elfouhaily, and B. Chapron, "Polarization ratio for microwave backscattering from the ocean surface at low to moderate incidence angles," in *Proc. Int. Geoscience and Remote Sensing Symp. 1998*, Seattle, WA, 1998.

[28] F. T. Ulaby, R. K. Moore, and A. K. Fung, "Microwave remote sensing and surface scattering and emission theory," in *Chapter Introduction to Random Surface Scattering and Emission*. Reading, MA: Addison-Wesley, 1982, pp. 922–1033.

[29] T. Elfouhaily, D. R. Thompson, D. Vandemark, and B. Chapron, "A new bistatic model for electromagnetic scattering from perfectly conducting random surfaces," *Waves Random Media*, vol. 9, pp. 281–294, 1999.

[30] T. Elfouhaily, "Physical modeling of electromagnetic backscatter from the ocean surface; Application to retrieval of wind fields and wind stress by remote sensing of the marine atmospheric boundary layer," Dépt. d'Océanogr. Spatiale, l'Inst. Français Rec. l'Exploitation Mer (IFREMER), Plouzane, France, 1997.
[31] P. W. Vachon and F. W. Dobson, "Wind retrieval from radarsat sar images: Selection of a suitable C-band HH polarization wind retrieval model," *Can. J. Remote Sensing*, vol. 26, no. 4, pp. 306–313, 2000.
[32] P. Bally and K. Fellah, "Evaluation of the accuracy of the backscattering coefficient measurement in SAR data products," Tech. Note, Eur. Space Res. Technol. Center, Nordwijk, Netherlands, 1995.

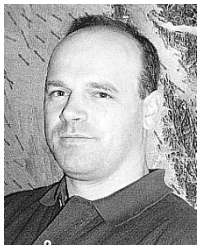

Jochen Horstmann received the Diploma degree in physical oceanography from the University of Hamburg, Hamburg, Germany, in 1997.

In 1995, he joined the Coupled Model System Group, GKSS Research Center, Geesthacht, Germany. In the framework of SARPAK, he worked on extraction of parameters from SAR. Since 2000, he has been a Research Scientist working in the ENVOC Project, GKSS Research Center. His research interests are in the extraction of wind fields from SAR. He is also working on algorithms to determine marine parameters from SAR images and application of interferometric SAR.

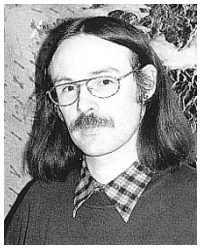

Wolfgang Koch received the state examination in mathematics, physics, and educational science from the University of Hamburg, Hamburg, Germany, in 1988.

He has been a Research Scientist with the Boundary Layer Grou, GKSS Research Center, Geesthacht, Germany, since late 1987. He has participated in numerous wave modeling projects, worked in verification of wind and wave measurements with altimeter, and is currently in the Coupled Model System Group working on wind estimation from SAR images.

Susanne Lehner received the M.Sc. degree in applied mathematics from Brunel University, Uxbridge, U.K., in 1979, and the Ph.D. degree in geophysics from the University of Hamburg, Hamburg, Germany, in 1984.

She was a Research Scientist, Max-Planck Institute for Climatology, Hamburg, Germany, and joined the German Aerospace Center (DLR/DFD), Oberpfaffenhofen, Germany, in 1996. Currently, she is a Research Scientist in marine remote sensing, Remote Sensing Technology Institute (DLR/IFM), Oberpfaffenhofen, working on the development of algorithms determining marine parameters from SAR.

Rasmus Tonboe received the M.Sc. in geology from the University of Aarhus, Aarhus, Denmark, in 1997.

Since 1997, he has been a Scientist with the Ice and Remote Sensing Division, Danish Meteorological Institute, Copenhagen, Denmark. His current research interests are in sea ice detection and description using satellite microwave data and extraction of wind fields from SAR data.